J. Fluid Mech. (1992), *vol.* 234, *pp.* 317–327
Printed in Great Britain

A finite-element method for inertial waves in a frustum

By GARY A. HENDERSON AND KEITH D. ALDRIDGE
Centre for Research in Earth and Space Science, York University, 4700 Keele Street, North York, Ontario M3J 1P3, Canada

(Received 18 September 1989 and in revised form 28 February 1991)

A finite-element method has been developed to model inertial waves in a frustum of a cone, since analytical methods have proved inadequate. The governing Poincaré problem is posed as a variational principle and approximate eigensolutions are computed. The numerical results are used to complete the interpretation of the experimental results of Beardsley (1970) for a frustum of a cone. The significant role played by characteristic surfaces partly explains the enigmatic nature of the ill-posed boundary-value problem that describes inertial wave resonances.

1. Introduction

An inertial wave is a periodic disturbance or normal mode of an incompressible fluid that is rotating almost rigidly in a container. A stationary observer sees the flow as an inward–outward faster–slower vortex. The low-order modes with simple structure are easily excited and may occur spontaneously even in situations not designed for them. For instance, these fluid modes are of some concern in the fields of aerospace and ballistics.

It is not unusual for a space vehicle or artillery shell to hold a liquid-filled tank and to be spin-stabilized. These features are contradictory and can cause the satellite or projectile to tumble out of control. It was shown by Stewartson (1959) that the rotation of a top containing liquid may become unstable when the nutation of the container and an oscillation of the liquid are nearly resonant. The nutation acts as a forcing for the oscillation which is thus steadily excited. If the container imparts some energy to the liquid, then reciprocally the liquid must exert a torque on the container. The oscillation acts simultaneously as a forcing for the nutation which is thus divergent. This effect of inertial waves has been the subject of recent studies by Pohl (1984) and Murphy (1986), etc. A remedy might well be to ascertain what sort of tank avoids sloshing fluid.

The role of rotation in geophysical fluid dynamics has been well known for both the atmosphere and oceans. The dynamics of the Earth's fluid core have recently also been studied in this context by Aldridge, Lumb & Henderson (1989), and for this application the importance of an irregular boundary has been realized. The present work is a first step toward understanding what happens to the inertial wave spectrum when a rotating fluid is in a conical cavity.

A global inertial wave belongs to a set of distinct eigenmodes with a discrete spectrum of eigenfrequencies, but not every shape of cavity allows these in a fluid. This inconsistency is reflected in the mathematics. The governing differential equation and boundary condition together constitute the so-called Poincaré problem. The differential equation is one of the hyperbolic type with characteristic lines that

lie in conical surfaces and have frequency dependent slope. The boundary condition is generally not one of the types usually applicable. This peculiar combination means that the existence of any eigensolutions is sensitive to the geometry of the boundary. That is, the problem is ill-posed as pointed out by Stewartson & Rickard (1969). This entails intractability, and analytical methods are generally inadequate except for a few cases. A separation of variables was successful for Kelvin (1880) or Bryan (1889), but current interest is in less regular geometries than cylinders or spheres. Consequently, recourse must be had to numerical methods for most cases. An approximate algebraic problem may then be solved instead.

There are at least two precedents for computational models of inertial waves on the basis of variational principles. For instance, Aldridge (1972) applied a classical Ritz method, whereas McIntyre & Tanner (1987) applied a modern finite-element Ritz method. The latter approach is also taken below in much the same way, but there is little comparison with regard to emphasis and cases. In particular, how the numerical method responds to a case where no eigensolutions exist has not been addressed before. The overall conclusion is that for axisymmetric geometries the Poincaré problem is well suited to the finite-element method and accurate approximations for low-order eigensolutions may be obtained with coarse meshes.

A family of three geometries is considered in turn. First, the cylinder is a benchmark case where the eigensolutions are well known. Greenspan (1968) reviewed analytical expressions for the eigenfrequencies and eigenfunctions that can both be referred to for verification. Secondly, the frustum is a practical case where the eigensolutions are barely known. Beardsley (1970) discovered experimental evidence for at least three eigenfrequencies and inferred that the eigenfunctions are deformations of those for a cylinder. The identification of these resonances as distorted inertial waves has not previously been confirmed by theoretical results. Thirdly, the cone is an exceptional case where the eigensolutions are likely non-existent. Greenspan (1969) theoretically predicted that no global eigenmodes would be found because the energy of any local disturbances would be repeatedly reflected along the characteristic lines toward the apex that acts as a sink. Beardsley (1970) experimentally verified both the absence of eigenmodes and the manifestation of characteristic lines. The similar lack of any eigensolutions has not previously been confirmed by attempting to solve the problem.

2. Method

Poincaré (1910) shows that for inertial waves the governing problem is

$$\nabla\cdot\nabla\Phi-(4/\lambda^2)\,\nabla\cdot\hat{\boldsymbol{k}}\hat{\boldsymbol{k}}\cdot\nabla\Phi=0, \tag{1}$$

$$\hat{\boldsymbol{n}}\cdot\nabla\Phi-(4/\lambda^2)\,\hat{\boldsymbol{n}}\cdot\hat{\boldsymbol{k}}\hat{\boldsymbol{k}}\cdot\nabla\Phi=(2/\mathrm{i}\lambda)\,\hat{\boldsymbol{n}}\cdot\hat{\boldsymbol{k}}\times\nabla\Phi, \tag{2}$$

which consists of a differential equation and accompanying boundary condition. It is assumed that inertia dominates viscosity and nonlinearity so damping and interaction of modes are negligible. The domain is a volume τ bounded by a surface Σ where a variable unit vector $\hat{\boldsymbol{n}}$ defines an outward normal. A constant unit vector $\hat{\boldsymbol{k}}$ defines the rotation axis. The dimensionless eigenfunction Φ is the amplitude of the reduced pressure. A temporal dependence $\propto\exp(\mathrm{i}\lambda t)$ has already been separated. The dimensionless eigenfrequency λ is confined to the bandwidth $0<|\lambda|<2$ and is pure real. This is discussed in more detail by Greenspan (1968).

The Poincaré problem posed equivalently as a variational principle is

$$\delta\mathscr{L}[\Phi]=0 \tag{3}$$

which expresses that the functional $\mathscr{L}[\phi]$ is stationary about each extremal Φ sought. This formulation reveals that the differential equation is an Euler one and that the boundary condition is a natural one. The functional is derived in much the same way as by Smylie & Rochester (1986). A general form that follows from the linear Hermitian operator is

$$\mathscr{L}[\phi] = \frac{(\mathrm{i}\lambda)^2}{2\pi}\int \phi^* \mathrm{L}\phi \,\mathrm{d}\tau \quad \text{where} \quad \mathrm{L} = \nabla^2 - \frac{4}{\lambda^2}(\hat{\boldsymbol{k}}\cdot\nabla)^2, \tag{4}$$

but a particular form can be obtained by enforcing the boundary condition. Hence, for the whole problem an appropriate functional is

$$\mathscr{L}[\phi] = \frac{1}{2\pi}\int (\lambda^2(\nabla\phi^*\cdot\nabla\phi) - 4(\nabla\phi^*\cdot\hat{\boldsymbol{k}}\hat{\boldsymbol{k}}\cdot\nabla\phi))\,\mathrm{d}\tau + \frac{\mathrm{i}\lambda}{\pi}\int (\phi^*(\hat{\boldsymbol{k}}\times\nabla\phi)\cdot\hat{\boldsymbol{n}})\,\mathrm{d}\Sigma, \tag{5}$$

since the extremals will satisfy both requirements of an eigensolution.

A scaled system of cylindrical polar coordinates (r, θ, z) is adopted. It is a simplification to assume an axisymmetric domain. An azimuthal dependence $\propto \exp(\mathrm{i}k\theta)$ is separated so the domain becomes a surface σ bounded by both a curve l and the z-axis. Hence, the functional and boundary condition are

$$\mathscr{L}[\psi] = \int\left[\lambda^2 r\left(\frac{\partial\psi}{\partial r}\right)^2 - (4-\lambda^2)\,r\left(\frac{\partial\psi}{\partial z}\right)^2 + \frac{k^2\lambda^2}{r}\psi^2\right]\mathrm{d}\sigma + 2k\lambda\int(\hat{\boldsymbol{r}}\cdot\hat{\boldsymbol{n}})\,\psi^2\,\mathrm{d}l, \tag{6}$$

$$\lambda^2\left((\hat{\boldsymbol{r}}\cdot\hat{\boldsymbol{n}})\frac{\partial\psi}{\partial r} + (\hat{\boldsymbol{k}}\cdot\hat{\boldsymbol{n}})\frac{\partial\psi}{\partial z}\right) + \lambda(\hat{\boldsymbol{k}}\cdot\hat{\boldsymbol{n}})\frac{2k}{r}\psi - 4(\hat{\boldsymbol{k}}\cdot\hat{\boldsymbol{n}})\frac{\partial\psi}{\partial z} = 0, \tag{7}$$

where the trial function ψ depends on two coordinates (r, z) only. The $r = 0$ singularity imposes the artificial boundary condition that $\psi = 0$ or $\partial\psi/\partial r = 0$ along the z-axis when $k > 0$ or $k = 0$ respectively.

The low-order extremals of the functional are obtained by resorting to a finite-element Ritz method, which is discussed in more detail by Davies (1980) and others. First, in accordance with the Ritz method, a trial function is expanded as a series of chosen basis functions combined by unknown weights. This is a truncation of the problem, since only a limited number of degrees of freedom are admitted. The extremals are found by optimization of the adjustable weights for fixed basis functions. Secondly, in accordance with the finite-element method, the basis functions are chosen piecewise so each exists over a subdomain but vanishes elsewhere. The extremals are found as patchworks after dividing the domain into a mesh of elements connected at nodes. Accordingly, for substitution into the functional the trial function is

$$\psi = \sum_i \sum_e N_i^e \delta_i \tag{8}$$

where $N_i^e(r, z)$ is a basis function to be defined on the eth element and δ_i is the ith weight to be found. This is a superposition over each element and a juxtaposition over the whole mesh. There is almost a dissection of the problem, but the pieces are weakly coupled through the weights.

Figure 1 shows three example meshes, one for each case considered. The meshes are composed in large measure of rectangular elements, but with an admixture of triangular elements wherever the boundary slopes. It is best that a mesh of elements be a complete reconstruction of the original domain. The rectangular elements each

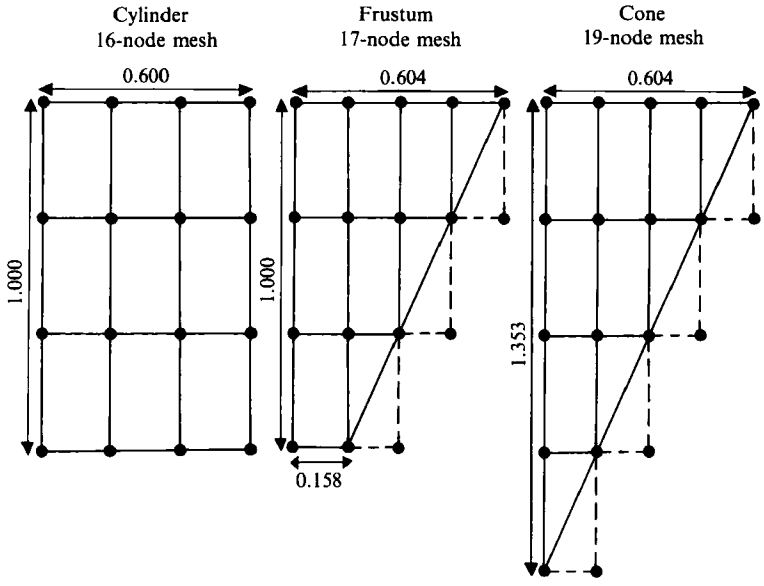

FIGURE 1. An example of meshes for the cylinder, frustum and cone.

have four proper nodes located at the vertices. These are just standard Quad4 elements. The triangular elements each have three proper nodes located at the vertices, but also one virtual node imagined at the missing vertex. These are *ad hoc* half-Quad4 elements, as opposed to standard Tria3 elements. The two sorts of elements chosen are compatible.

The basis functions are chosen so that each weight denotes the value of either the trial function ψ or one of its derivatives $\psi_r, \psi_z, \psi_{rz}$ at some nodal point. In this way most weights have physical significance and pieces of the trial function are coupled. A basis function N_i^e exists only if the ith weight δ_i corresponds with any node of the eth element. There are sixteen i associated with each e, but up to four e associated with each i as well. The basis functions are piecewise bicubic Hermite interpolation polynomials, which ensure that the extremals obtained are continuous and smooth even between the elements.

The ensuing algebraic problem is

$$\boldsymbol{K}\boldsymbol{\delta} = 0, \tag{9}$$

where $\boldsymbol{K}$ is a matrix of coefficients and $\boldsymbol{\delta}$ is a vector of weights. This arises since the functional (ψ, ψ) is a quadratic form and partial derivatives with respect to the weights must vanish. In terms of the frequency the coefficient matrix is

$$\boldsymbol{K} = \lambda^2 \boldsymbol{A} + \lambda \boldsymbol{B} + \boldsymbol{C}, \tag{10}$$

where as a rule the numerous entries are

$$\left.\begin{aligned} A_{ij} &= \sum_e \int \left(r \frac{\partial N_i^e}{\partial r} \frac{\partial N_j^e}{\partial r} + r \frac{\partial N_i^e}{\partial z} \frac{\partial N_j^e}{\partial z} + \frac{k^2}{r} N_i^e N_j^e \right) \mathrm{d}\sigma^e, \\ B_{ij} &= 2k \sum_e \int (\hat{\boldsymbol{r}} \cdot \hat{\boldsymbol{n}}) N_i^e N_j^e \, \mathrm{d}l^e, \\ C_{ij} &= -4 \sum_e \int r \frac{\partial N_i^e}{\partial z} \frac{\partial N_j^e}{\partial z} \mathrm{d}\sigma^e, \end{aligned}\right\} \tag{11}$$

although some rows are replaced to explicitly enforce the boundary conditions at the peripheral nodes. If k is zero then $\boldsymbol{B}$ is a zero matrix. The closing frequency restriction is

$$|\lambda^2\boldsymbol{A}+\lambda\boldsymbol{B}+\boldsymbol{C}| = 0, \tag{12}$$

which is that the determinant of the coefficient matrix must vanish for a non-trivial vector of weights to exist.

Therefore, the low-order eigenfrequencies are obtained as the roots of some secular equation, and the corresponding eigenvectors of weights are obtained as the solutions of systems of linear homogeneous equations. A few eigenfunctions are plotted at additional points in each element by interpolation between the nodes from the weights and basis functions. The secondary numerical methods used to solve the algebraic problem are kept quite straightforward.

The coefficient matrix is large, on the order of 100×100 entries, but sparse. A narrow diagonal band contains all the non-zero entries or information, so this alone is stored and manipulated. The entries of the coefficient matrix are sums of symmetric bilinear forms (N_i^e, N_j^e), which are double integrals with integrands that are polynomials or rational functions. The majority, due to rectangular elements, are evaluated from general expressions when reduced by factorization and analytical integration. The remainder, due to triangular elements, are evaluated or estimated by numerical quadrature with 7- or 16-point Gauss–Legendre formulas.

The determinant of the coefficient matrix is some high-degree polynomial function of the frequency. To find the zeros of such a pathological function is tricky. The roots are located using the bisection method, which is orderly and infallible for isolated single roots in a fixed bandwidth. At each frequency sampled the sign of the determinant is found using Gaussian elimination with scaled column pivoting. Any propagation of rounding error due to ill-conditioning does not appear fatal. An eigenvector of weights is obtained, once the corresponding eigenfrequency is located, by back-substituting the coefficient matrix which is in upper triangular form.

The freedom or resolution of the trial function is dependent on the number of nodes or elements in the mesh. As the mesh is gradually refined there ought to be an increase in the accuracy and number of eigensolutions obtained so that previous ones are improved while additional ones are introduced. Hence, it is the eigensolutions with the simplest structure that tend to be obtained the earliest and best. A succession of approximations for the same eigensolution ought to be either convergent or spurious.

3. Results

The eigenmodes are identified with integers (m, k, n) which loosely stated are the (radial, azimuthal, vertical) wavenumbers. These indicate how low the order of complexity in the structure of an eigenfunction is with respect to each direction. The eigenfunctions by nature are each distinctively organized into various cells. For all the cases considered, $k = 0$ means the cells are axisymmetric, while m and n denote respectively how many cell walls are crossed by a line drawn radially or vertically.

The first case considered is a cylinder. This is required for verification of the numerical method. A comparison is made between the eigenfrequencies obtained and those known from an expression derived by Kelvin (1880), and confirmed by the pattern of cells in the eigenfunction obtained. The eigensolutions recovered are those with the smallest wavenumbers, and those of lower order do tend to have higher

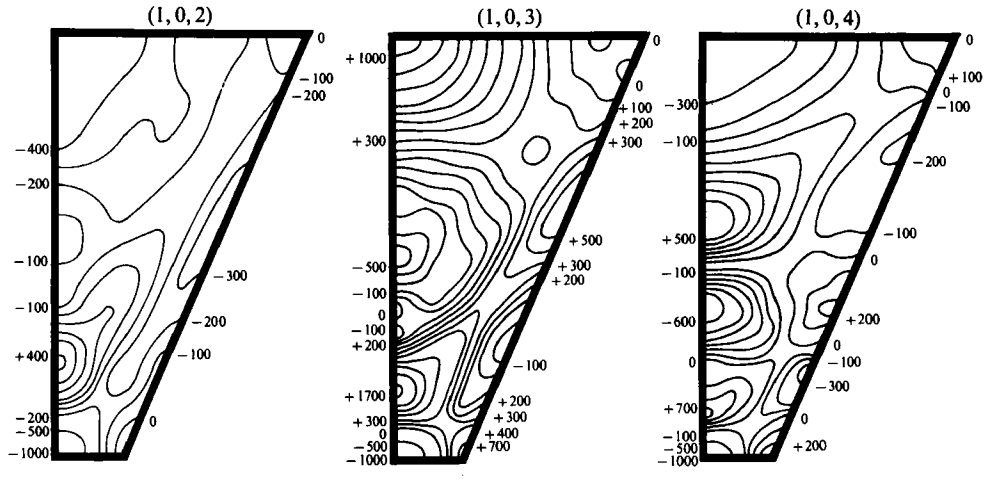

FIGURE 2. The isobar charts of the eigenfunctions obtained for the frustum with an 80-node mesh.

Nodes	λ_{102}	λ_{103}	λ_{104}
11	1.1723	1.3821	1.5597
48	1.1219	1.3310	1.5141
67	1.1165	1.3252	1.5098
80	1.1187	1.3277	1.5154
94	1.1190	1.3274	1.5160
Numerical	1.12	1.33	1.52
Experimental	1.12	1.30	1.48

TABLE 1. The eigenfrequencies recovered for a frustum

accuracy. As the mesh is refined along an axis the eigensolutions recovered do include additional ones with larger wavenumber and previous ones with improved accuracy. Thus there is convergence, and very rapidly. A 25-node mesh is enough to recover several low-order eigenfrequencies within 0.1% tolerance and the eigenfunctions with somewhat less accuracy. In short, the numerical method behaves as predicted.

The second case considered is a frustum. There are three or four resonant frequencies distinctly revealed in the experimental data of Beardsley (1970). An 11-node mesh allows the numerical method to recover none other than four comparable eigenfrequencies in that bandwidth. This coincidence shows that the numerical method and experimental process are compatible since both have a low-order bias. Whether a study is experimental or numerical, the eigenmodes with the simplest structure are the easiest to excite or recover. It is convenient to locate these eigenfrequencies with a coarse mesh and then track them through several refinements.

At the top of table 1 three sequences of like eigenfrequencies recovered with various meshes are shown. The frustum requires a more refined mesh than the cylinder to recover low-order eigenfrequencies as accurately. Thus there is convergence, but less rapidly. This is predictable to the extent that the problem is less well-posed for a frustum than for a cylinder. At the bottom of table 1 a comparison between the numerical and experimental estimates of these eigenfrequencies is shown. Of course, the numerical values are those the method

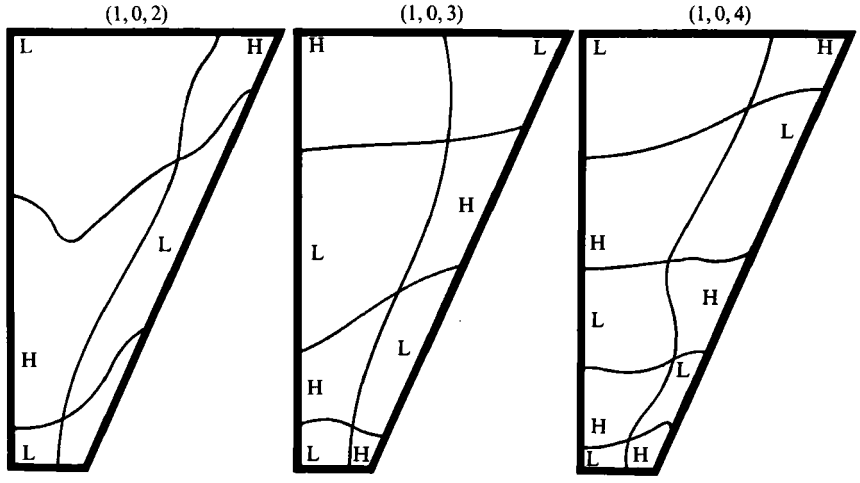

FIGURE 3. The cell charts of the eigenfunctions obtained for the frustum.

converged to, and the experimental values are those reported by Beardsley (1970). These values are practically the same, since the latter are all uncertain by a few units in the second decimal place.

It is apparent that at least in principle the eigensolutions for the frustum are perturbations of those for a cylinder. A footnote of Beardsley (1970) remarks that both phase and amplitude measurements suggest the resonance at $\lambda = 1.12$ is probably a distorted $(1, 0, 2)$ eigenmode even though the side leans sharply. Figure 2 shows isobar charts of the three eigenfunctions obtained with an 80-node mesh. It is clear that in each chart the isobars divide naturally into several cells and that in each cell the isobars mark a relative low or high. Figure 3 shows cell charts of the three eigenfunctions. It seems from many cell charts that the eigenfunctions for the frustum may consist of peculiar adaptations to that shape as well as perturbations or truncations of those for a cylinder. However, there is an analogy between the structure of the predominant eigenfunctions for both geometries. The three eigensolutions obtained for the frustum are surely perturbations of the $n = 2, 3, 4$ members in the series of $(1, 0, n)$ eigensolutions known for a cylinder. It is notable that the high-order eigenfunctions in this series for the frustum are the least distorted and so the most like their counterparts for a cylinder. Moreover, the low-order eigenfunctions obtained suggest a few characteristic lines and possible discontinuities.

A perturbed $(1, 0, 1)$ eigenmode is conspicuous by its absence. This stresses that the similarity between the frustum and a cylinder is not complete. The experimental data of Beardsley (1970) has no evidence for a perturbed $(1, 0, 1)$ eigenmode, since the three chief resonances are all otherwise identified. A possible explanation is that damping of the fundamental eigenmode is much enhanced by the deformation going from a cylinder to a frustum. This same effect is seen going from a sphere to a shell in the experimental data of Aldridge (1967). The numerical method also leads to no evidence for a perturbed $(1, 0, 1)$ eigensolution, unless the bottom radius is increased to more than roughly 60% of the top one. A small relative amplitude cannot be confirmed since viscosity is neglected.

There is an elegant procedure to generate potential eigenfrequencies by ray tracing along special characteristic lines as demonstrated by Høiland (1962). A similar

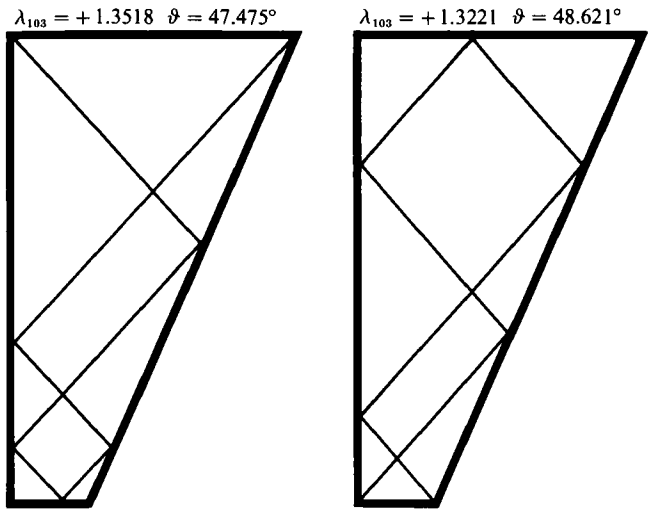

FIGURE 4. An example of tracing characteristics to estimate an eigenfrequency for the frustum.

geometrical method is used to estimate the perturbed $(1, 0, n)$ eigenfrequencies by tracing two special paths each consisting of $2n$ characteristic line segments. An example of this technique for the perturbed $(1, 0, 3)$ eigenfrequency is shown in figure 4. A slightly different estimate of the eigenfrequency is inferred from the slope of the line segments in each path. The eigenfrequencies obtained by this geometrical method and by the numerical method are in close agreement up to $n = 7$ at least. There is no discrepancy greater than 0.06, and the spread decreases as n increases. The perturbed $(1, 0, 1)$ eigenfrequency is again an exception, since it is not possible to trace the first path with just two line segments.

The third case considered is a cone. Beardsley (1970) remarks that both phase and amplitude measurements indicate an absence of any eigenmodes. The perturbed $(1, 0, 2)$ eigensolution is singled out and revealed by the numerical method as bogus. This is suggested by a sequence of like eigenfrequencies generated with several meshes. The cone seems to require a much more refined mesh than even a frustum to obtain the eigenfrequency with the same accuracy. Thus there is not proper convergence, and the eigensolution is not genuine. This is emphasized by the corresponding sequence of unlike eigenfunctions generated. As the mesh is refined the evolving structure of the supposed eigenfunction is eventually not at all of the sort predicted. An isobar chart of the spurious eigenfunction generated with a 64-node mesh is shown in figure 5.

The characteristic lines evident in this isobar chart are shown in figure 6. There is a narrow diagonal band in the middle that clearly shows the upward sloping characteristics. There is a large diagonal band at the top that clearly shows the downward sloping characteristics. It also appears that in a sense the downward characteristics are crossing over and interfering with the upward characteristics to create cells nearly the size of the elements. At a slightly lower frequency the upward characteristics would be parallel with the boundary. It seems the spurious eigensolution generated is tending towards that limit and ever smaller cells as the mesh is refined.

It is desirable to find how the $(1, 0, 2)$ eigenmode fails to complete the transition from frustum to cone. The mesh is gradually changed to draw the frustum to a point

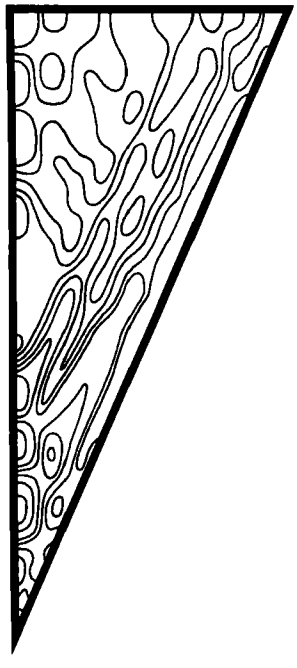

FIGURE 5

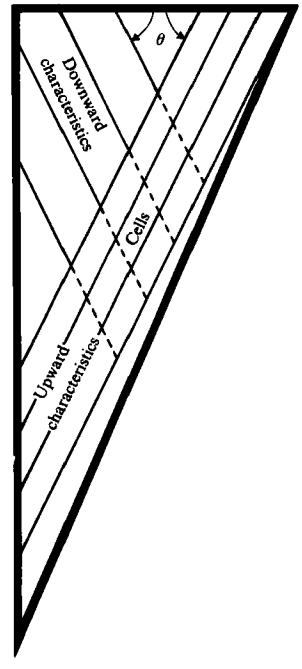

FIGURE 6

FIGURE 5. An isobar chart of the eigenfunction generated for the cone with a 64-node mesh.
FIGURE 6. The characteristics observed in the isobar chart for the cone.

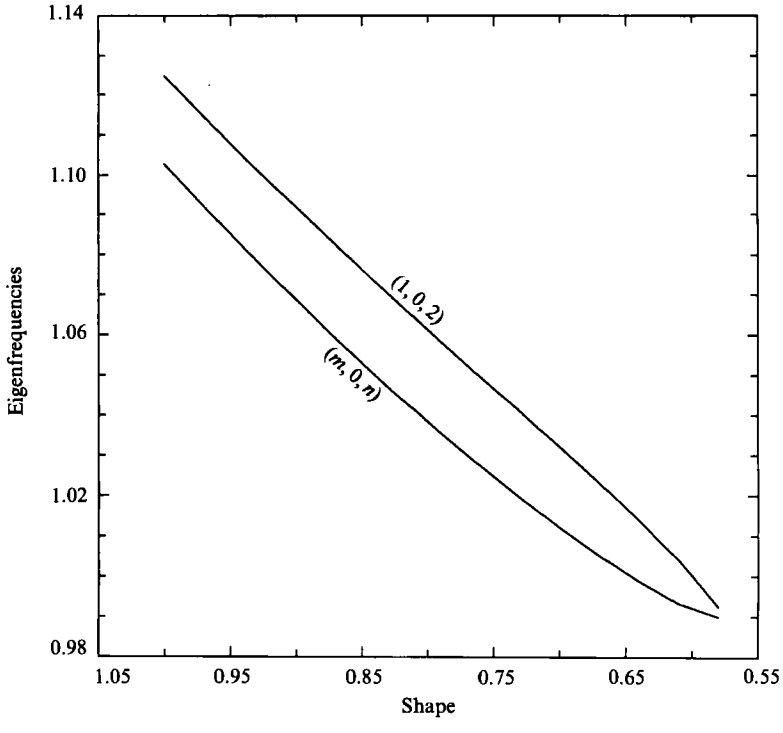

FIGURE 7. The disappearance of the eigenfrequency at the critical shape with a 38-node mesh.

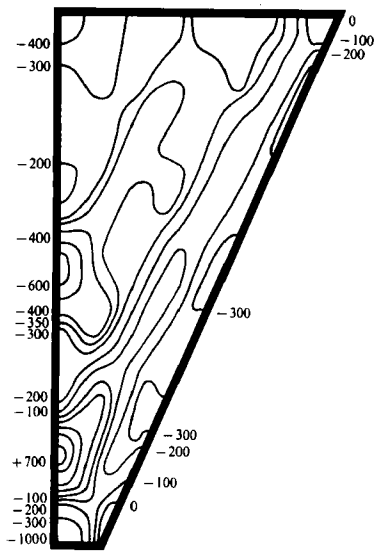

FIGURE 8. An isobar chart of the eigenfunction obtained for the critical shape with a 38-node mesh.

but is not refined overall. A ratio of the bottom radii is used as a measure of the shape, which assigns the value of unity to the original frustum and of zero to the cone. As the shape is lowered the magnitudes of the eigenfrequencies are also generally decreased. However, there is a critical shape below which the (1, 0, 2) eigenfrequency suddenly disappears. Figure 7 shows the disappearance of the eigenfrequency and its companion when tracked with a 38-node mesh. A mathematical explanation for this may be inferred. The eigenfrequency is one of a pair of zeros that bracket a local maximum of a secular polynomial. As the critical shape is approached, the plateau falls toward the axis and the zeros move closer together, until abruptly the plateau falls below the axis and both zeros disappear.

A coarse mesh might not be able to resolve much of the difference between an almost critical shape and the cone. As the mesh is refined the critical shape tends to grow more pointed. However, it is not clear whether the limit of the critical shape is the cone. Figure 8 shows an isobar chart of the eigenfunction obtained for the critical shape with a 38-node mesh. The cells and characteristics that are the main features of the isobar charts for the original frustum and cone are combined.

The above results are a significant supplement to those of Beardsley (1970). It has been shown that a basic use of a numerical method leads to insight for classic cases of the Poincaré problem. Specifically, a theoretical model of inertial waves has been used to clarify a pair of experiments after a long hiatus. This type of study has been hindered by the difficult mathematical problems, but the advent of finite-element methods promises a revival.

This work was generously funded in part by an operating grant from the NSERC of Canada, a scholarship from the province of Ontario and a fellowship from Allied-Signal Canada Inc. The authors are grateful to Dr M. E. McIntyre for helpful suggestions.

REFERENCES

ALDRIDGE, K. D. 1967 An experimental study of axisymmetric inertial oscillations of a rotating liquid sphere. PhD dissertation, M.I.T.

ALDRIDGE, K. D. 1972 Axisymmetric inertial oscillations of a fluid in a rotating spherical shell. *Mathematika* **19**, 163–168.

ALDRIDGE, K. D., LUMB, L. I. & HENDERSON, G. A. 1989 A Poincaré model for the Earth's fluid core. *Geophys. Astrophys. Fluid Dyn.* **48**, 5–23.

BEARDSLEY, R. C. 1970 An experimental study of inertial waves in a closed cone. *Stud. Appl. Maths.* **49**, 187–196.

BRYAN, G. H. 1889 The waves on a rotating liquid spheroid of finite ellipticity. *Phil. Trans. R. Soc. Lond.* A **180**, 187–219.

DAVIES, A. J. 1980 *Finite Element Method: A First Approach.* Clarendon.

GREENSPAN, H. P. 1968 *The Theory of Rotating Fluids.* Cambridge University Press.

GREENSPAN, H. P. 1969 On the inviscid theory of rotating fluids. *Stud. Appl. Maths* **48**, 19–28.

HØILAND, E. 1962 Discussion of a hyperbolic equation relating to inertia and gravitational fluid oscillations. *Geofys. Publ.* **24**, 211–227.

KELVIN, LORD 1880 Vibrations of a columnar vortex. *Phil. Mag.* **10**, 155–168.

MCINTYRE, J. E. & TANNER, T. M. 1987 Fuel slosh in a spinning on-axis propellant tank: an eigenmode approach. *Space Commun. Broad.* **5**, 229–251.

MURPHY, C. 1986 Stability of liquid-filled projectiles with unusual coning frequencies. *Report BRL-MR-3530*, Ballistic Research Laboratories.

POHL, A. 1984 Dynamic effects of liquid on spinning spacecraft. *Proc. First INTELSAT/ESA Symp. on the Dynamic Effects of Liquids on Spacecraft Attitude Control.*

POINCARÉ, H. 1910 Sur le précession des corps déformables. *Bull. Astronomique* **27**, 321–356.

SMYLIE, D. E. & ROCHESTER, M. G. 1986 A variational principle for the subseismic wave equation. *Geophys. J. R. Astr. Soc.* **86**, 553–561.

STEWARTSON, K. 1959 On the stability of a spinning top containing liquid. *J. Fluid Mech.* **5**, 577–592.

STEWARTSON, K. & RICKARD, J. A. 1969 Pathological oscillations of a rotating fluid. *J. Fluid Mech.* **35**, 759–773.